Thylakoids: from molecular to membrane organisation

Streckaite, S.

2021

document version
Publisher's PDF, also known as Version of record

Chapter 7

Thylakoid membrane imaging by PRN

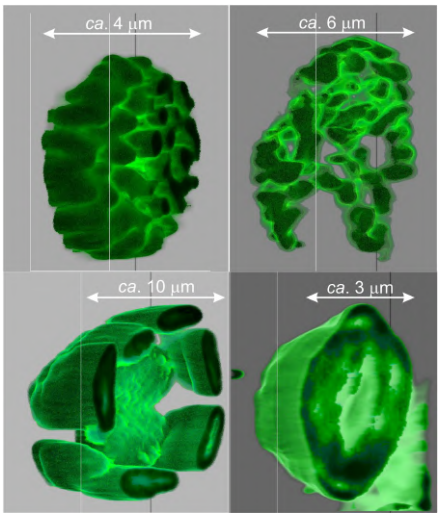

Abstract

Photosynthetic organisms must constantly adapt to their greatly varying light environments to ensure their proper energetic balance. This involves structural reorganisations at different levels of the organism, which tune the fate of the absorbed solar energy in the photosynthetic membranes. However, mechanisms behind this flexibility of photosynthetic organisms remain only partly understood. A number of molecular events related to non-photochemical quenching and state transitions have been characterised, but the precise description of these changes at the membrane level is still missing due to technical limitations to visualise thylakoids *in vivo* at physiological conditions. Most common approaches to image thylakoid membranes comprise diffraction-limited confocal microscopy techniques, and super-resolution fluorescence imaging, such as, structured illumination microscopy (SIM). Conventional fluorescence microscopy does not give access to nanoscopic scale due to limited resolution, in comparison to super-resolution techniques. However, the latter have technical limitations as discussed in Chapters 1 and 6, especially, compatibility with live samples. As a solution for diffraction-limited fluorescence microscopy and the complexity of the current super-resolution imaging techniques, a relatively simple and cheap light nanoscopy method is PRN, presented in detail in Chapter 6. This method enables us to study labelled compartments in cells, and even naturally fluorescent photosynthetic systems *in vivo* at physiological temperatures. The following study focuses on ap-

plications of PRN for visualization and 3D reconstruction of thylakoid membrane network in a variety of fluorescing photosynthetic organisms (plants, algae, diatoms).

7.1 Introduction

The fascinating adaptation of photosynthetic organisms to their enormously varying environments attract considerable interest from scientists from different backgrounds. This adaptation is achieved by structural reorganizations at various levels, as discussed in section 1.1.4. Thylakoid membrane architecture is quite diverse among different organisms (discussed in section 1.1.3), and yet photosynthesis is optimized in all of them[1]. Despite our deep knowledge in photosynthesis, 3D dynamics of these processes remain unexplored due to technological limitations related to investigation of the intraorganellar mechanisms *in vivo*.

Since the invention of electron microscopy (EM) in 1930s, the special organization of thylakoid membranes in photosynthetic organisms was mostly examined by this technique[2]. As discussed in section 1.1.3, thylakoid membranes in plant chloroplasts are organized into two morphologically and functionally different domains called grana and stroma. The way how these domains join together to form a continuous membrane system has been the subject of study for several decades, and the EM-based studies have led to a variety of 3D models. The first and most popular helical model[3] describing the thylakoid architecture in plants states that each grana is surrounded by multiple stroma lamellae wrapping around the grana as right-handed helices. The latest 3D model was also obtained from the EM measurements and declares a more complicated structure with the stroma lamellae wounding around grana in both directions – the network is stabilized by arrays of right- and left-handed helical structures[4]. However, as these models are based on EM studies, they represent snapshots of highly treated samples and do not capture the dynamics of the thylakoid system. The structures of thylakoid network in their native state exist as 3D models for plants chloroplasts, however, for other photosynthetic organisms there are no such models yet.

Another widely studied organism is the unicellular green alga *Chlamydomonas reinhardtii* (*r.*), which is a model organism for photosynthesis, chloroplast biology, cell cycle control, genetic studies[5–8], etc. As it is shown by EM[9] in Fig. 1.6C, it has an oval shape and is approximately as twice the dimensions of plant chloroplasts shown Fig. 1.6B. *Chlamydomonas r.* possess a single-cup shaped chloroplast that occupies more than half of the cell volume. At the opposite end than the flagella, *Chlamydomonas r.* have pyrenoid – the site of CO_2 fixation, where the enzyme Rubisco is concentrated. In plants, Rubisco is homogeneously distributed through the stroma[9–11]. Despite the tremendous studies performed on this green alga, the 3D ultra-structure of thylakoid network *in vivo* has not been obtained yet. This is also true for another photosynthetic organisms gaining more and more attention lately – diatoms. They are very interesting due to the sophisticated cell ultrastructure: diatoms possess nanostructured hard silica-based outer-shell. A vast variety of sizes and shapes of the shell structures of diatoms exist, exhibiting

photonic crystal properties[12]. Inside the shell of diatoms, few to many plastids can be found, depending on the species[13,14]. The attention from the photosynthesis point of view is drawn to their thylakoid organization, contrasting to the aforementioned organisms, which is composed of loose thylakoid membrane stacks[1,15], as shown by EM in Fig. 1.6D.

Detailed insights on the thylakoid organization in photosynthetic organisms were achieved with advanced derivatives of EM. Some examples include scanning-electron microscopy (SEM), which was applied for thylakoid membrane imaging of intact diatom *Phaeodactylum tricornutum* (*t.*) cells[13], transmission-electron microscopy (TEM), which was used to obtain a whole pea mesophyll cell[16], as well as their derivative, scanning-TEM (STEM), which was used to image chloroplasts in the lettuce mesophyll[4]. The most advanced EM techniques, enabling visualization of the cells and their compartments in 3D with a molecular resolution *in situ*, are electron tomography (ET) and cryo-electron-tomography (cryo-ET). The former was applied for detailed visualization of intact spinach chloroplast[17], and the latter showed unprecedented resolution in imaging the volume of *Chlamydomonas r.* cells[11]. Another interesting thylakoid images can also be found in the literature, for example, based on X-ray tomography which was used to obtain the 3D reconstruction of the *Chlamydomonas r.* cell[18].

However, EM techniques are not only limited by demanding set-ups, but also by a complex sample preparation, which requires chemical fixation, dehydration, staining, plastic embedding, mechanical stress[19]. Each of these steps can result in undesirable artefacts; they can distort labile chloroplast structures and which may no longer be biologically relevant. Therefore, we need to consider live-cell imaging conditions to visualize processes *in vivo* or in their close-to-native state. The best tool for that is fluorescence imaging due to natural chlorophyll fluorescence in thylakoids which can be used to observe them; thus no staining or additional protein expression methods are required.

Available techniques for fluorescence imaging are confocal microscopy and its derivatives, as well as super-resolution (SR) fluorescence imaging techniques. While the conventional fluorescence microscopy is fundamentally limited to the fine details of the size of approximately half of the excitation wavelength used, SR imaging overcomes this diffraction limit and push the resolution down to the nanoscale range (discussed in more detail in section 1.2.3). Successful attempts for thylakoid membrane imaging *in vivo* and *in situ* were provided by confocal laser-scanning microscopy (CLSM) – imaging of the intact pea chloroplast[16], super-resolution confocal live-imaging microscopy (SCLIM) – an intact *Arabidopsis thaliana* (*th.*) chloroplast[20], as well as three-dimentional structured illumination microscopy (3D-SIM), which was used for high-resolution imaging of mesophyll chloroplast of *Arabidopsis th.* and *Chlamydomonas r.* cell[21].

Although the resolution of SR techniques is lower than that of EM, the information ob-

tained *in vivo* in real-time on chloroplast dynamics is highly complementary and essential for the holistic understanding of thylakoid network function in ever-changing and challenging environments. The aim of this chapter is to apply the novel fluorescence imaging method, PRN, for photosynthesis in order to obtain 3D visualization of the thylakoid structure of an entire plant chloroplast and other model organisms in their *in vivo* or close-to-native states.

7.2 Results and discussion

7.2.1 Thylakoid organisation in intact plant chloroplasts

Figure 7.1A shows the 2D PRN images of different plant chloroplasts – the cross-sections at around the central plane. Also, for qualitative comparison, examples of arabidopsis imaged with SCLIM and 3D-SIM are shown in Fig.7.1B. It is known that LHCII-PSII complexes and LHCII trimers can be found exclusively in the bright areas, but a significant amount of PSI and PSII emissions are merged. Therefore, LHCI-PSI complexes might be located in both, dark and bright areas[16]. From Fig. 7.1 it can be observed that the size and shape of the fluorescent spots corresponding to the grana stacks, differ slightly between species. In agreement with previous studies, it is observed that pea chloroplasts exhibit less clear grana and stroma structures when compared to spinach and arabidopsis chloroplasts[16,22]. It is important to note that the emission observed is coming from the chlorophyll molecules within the thylakoids and not the membrane itself, which can give a slight mismatch from the boundaries of the membranes. Moreover, it is challenging to obtain clear images of the membrane network within the chloroplast due to very high concentrations of Chl pigments. As can be seen from Fig. 7.1, SCLIM shows poor visualization of the grana and stroma structures. Meanwhile PRN provides exceptional images with a very clear grana stacks, probably due to very good z-resolution of this method (Chapter 6).

For quantitative comparison of grana sizes, a reasonable amount of data is needed for statistical analysis from independent experiments performed under the exact same conditions. Such a study was performed for spinach chloroplasts grown under different illumination conditions: low and high-light (LL and HL, respectively); see Materials and methods (section 7.4) for more details. The grana stack diameter is defined as a full-width-at-half-maximum (FWHM) of the Gauss fit of the recorded image (see Materials and methods (section 7.4)). Grana diameters for two growth conditions for dark-adapted (DA) plants are shown in Fig. 7.2. For HL $\rightarrow$ DA we obtained 380 nm, and for LL $\rightarrow$ DA – 420 nm grana diameter. In agreement with plant adaptation behaviour discussed in section 1.1.4, reasonably larger grana diameters are observed for LL plants: for 5 times more intense light conditions grana diameter decrease by 10 % (by

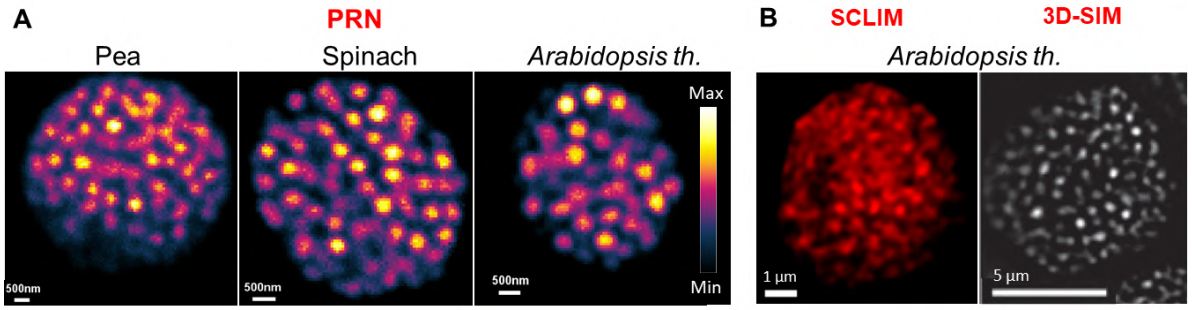

Fig. 7.1. Thylakoid organization in different plant chloroplasts. (A) PRN images of pea, spinach and arabidopsis. (B) Examples found in literature: super-resolution confocal live-imaging microscopy (SCLIM) and three-dimentional structured illumination microscopy (3D-SIM) images of arabidopsis for comparison. For PRN, pea was scanned by 80 nm *x&y* steps, with 60x objective, collecting emission in 675-685 nm range. Spinach and arabidopsis was scanned by 60 nm *x&y* steps, with 100x objective, collecting emission in 660-700 nm range. All samples were excited at 488 nm. (B, left) is reproduced from Iwai *et al.*, *Scientific reports*, 2016[20], (B, right) is reproduced from Iwai *et al.*, *The Plant Journal*, 2018[21].

40 nm). For similar LL spinach growth conditions (200 µEm^{-2}s^{-1}for 12 h/d) grana diameter was determined by SIM as 390 nm (LL $\rightarrow$ DA)[22]. It is possible that higher diameters (420 nm) observed by PRN in this work is due to the fact that plants were grown under less intense illumination (120 µEm^{-2}s^{-1}) for a shorter period (8 h of exposure).

Another example of grana diameter of 370 nm was shown for arabidopsis for similar growth conditions (100 µEm^{-2}s^{-1} of 9 h/d). It was obtained by confocal laser scanning microscopy (CLSM)[23], and this diameter value was later corrected by biochemical data as representing only *ca.* 70 % of the real grana diameter, because CLSM most likely detects the grana core only and not the margins. The reason for this might be the lower concentration of PSII (of *ca.* 50 %) in grana margins compared to grana core[24]. Therefore, as we are trying to observe structural changes, which occur in a few tens of nanometers in a rather densely packed membrane system, the use of confocal microscopy for grana evaluation studies might be limited due to low lateral resolution and very poor axial resolution. On the other hand, PRN shows satisfying results for such studies which, due to simplicity, could be a better choice when compared to other SR techniques.

7.2.2 3D reconstruction of arabidopsis thylakoid network

It is interesting that grana stacks are always oriented perpendicular to the surface the chloroplast is positioned on, as shown in Fig. 7.1, and the side view of thylakoid structure can be visualized only by the 3D reconstruction or by embedding chloroplasts in a medium, such as agarose[21]. Up to now, the only models available for the 3D visualization of thylakoid architecture in native chloroplasts/cells are obtained by CLSM for plants[16,25], and by SCLIM for moss[20]. In these

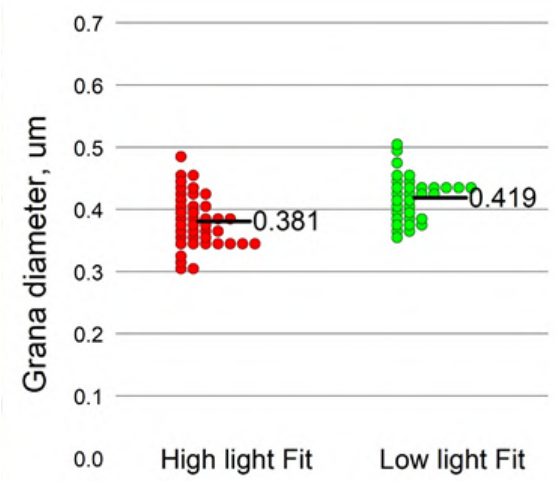

Fig. 7.2. Spinach grana diameter dependence on the plant growth conditions.

3D visualizations we cannot distinguish clear grana and stoma domains for pea, bean[16,25] and *Physcomitrella patens* (*p.*)[20], despite that in the 2D images it is evident (Fig. 7.3E). As was highlighted before, thylakoid organization is dependent on the species. Therefore, one might not expect to obtain a 3D thylakoid structure with well-separated grana and stroma thylakoids for a particular organism. However, for plants one would predict a somewhat more clearly defined membrane architecture. The 3D reconstructions shown in Fig. 7.3E were obtained by confocal microscopy – the low resolution can also be the reason for the poor visibility of the detailed thylakoid system.

The PRN method, yielding much higher resolution than confocal microscopy, was applied to obtain the 3D membrane structure of an arabidopsis chloroplast. Several 2D planes were scanned every 300 nm in z axis, as shown in Fig. 7.3A, and an almost whole (*ca.* 2 µm) chloroplast thylakoid network is obtained by 3D reconstruction. From the cross-sections of the volumetric structure (Fig. 7.3B) we can see that stacked areas are irregular, merging with each other and are not always parallel as typically depicted or modelled from EM data[17]. In this particular case, the chloroplast is deformed and not laying on a flat surface. If one looks at the spacial arrangement of the thylakoids from the side (every 140 nm in x direction) or slicing through the volume (every 180 nm in z direction) of the chloroplast (Fig. 7.3C and D, respectively), disordered connections between grana stacks can be seen. Nevertheless, grana stack appearances and disappearances can be followed together with stroma lamellae interconnections. This is shown in Fig. 7.3C, where the yellow dotted lines represent horizontally aligned grana stacks, meanwhile the pink dotted lines show stroma thylakoids. Following these lines in the image sequence, it is obvious that grana and stroma thylakoids form a continuous network within the chloroplast. Such a structure agrees with the helical model, where the stroma is connected at an angle to the grana[4,17,26,27]. However, it does not seem to wind around the grana and looks

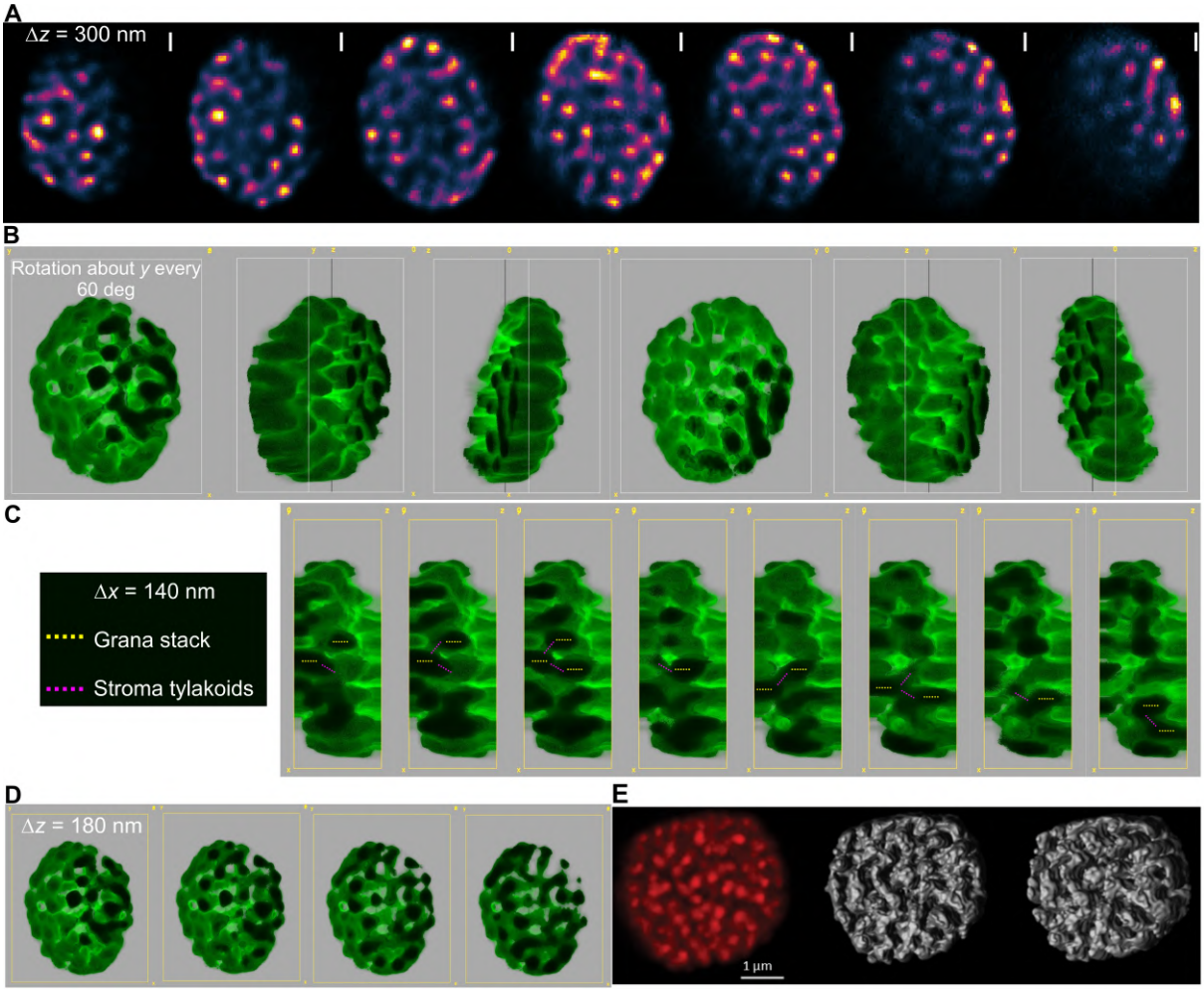

Fig. 7.3. (A) PRN images of an axial scan of arabidopsis chloroplast. (B) Cross-sections of the 3D reconstruction (obtained from the images shown in panel (A)) every 60 degrees around *y* axis. (C) Cross-sections of the 3D reconstruction from the side view every 140 nm in *x* direction. Grana and stroma lamellae continuous network is shown by following yellow (grana) and pink (stroma lamellae) lines in the sequential images. (D) Cross-sections of the 3D reconstruction slicing through the volume every 180 nm in *z* direction. (E) Examples found in literature: chlorophyll fluorescence recorded by CLSM from an intact pea chloroplast (red) and 3D reconstruction: face and side view (grey). In panel (A), vertical scale bar at the top right corner of the images is 500 nm. Chloroplast was scanned by 70 nm *x*&*y* steps, and 300 nm *z* steps, with 100x objective, collecting emission in 660-700 nm range. Sample was excited at 488 nm. Shown data was deconvolved as described in Materials and methods (section 6.4). Images in panel (E) are reproduced from Rumak et al, BMC Plant Biol., 2012 [16].

more as extensions connecting one grana with another. On the other hand, there is a lack of information on PSI emission, which could fill the empty spaces around grana, the chloroplast model proposed from EM studies cannot be proven or denied.

7.2.3 The *in vivo* thylakoid organisation in *Chlamydomonas r.*

As higher plants and green algae are considered to have similar photosynthetic apparatus, unravelling the thylakoid organization of the latter *in vivo* is of high interest. However, it is not an easy task, as the *Chlamydomonas r.* cell is approximately twice as big as a typical plant chloroplast, thus at the limit of most of the current SR imaging techniques. The advantage of the PRN method is the possibility to image relatively large volumes. The 2D PRN images of three *Chlamydomonas r.* cells at their middle plane are shown in Fig. 7.4. From these images, it should be emphasized that a wide variety of thylakoid membrane structures and overall appearances in different cells are observed even if they were from the same sample preparation (Fig. 7.4A). If we take a closer look at some regions (Fig. 7.4B), which PRN enables us to do by scanning the ROI by a smaller step as discussed in Materials and methods (section 6.4), it is observed that stack-like thylakoid membrane domains have some similarities to the membrane stacks in plants. They are not that well organized, but also resemble the concentration of different pigment-protein complexes in the stacked and loose regions[28].

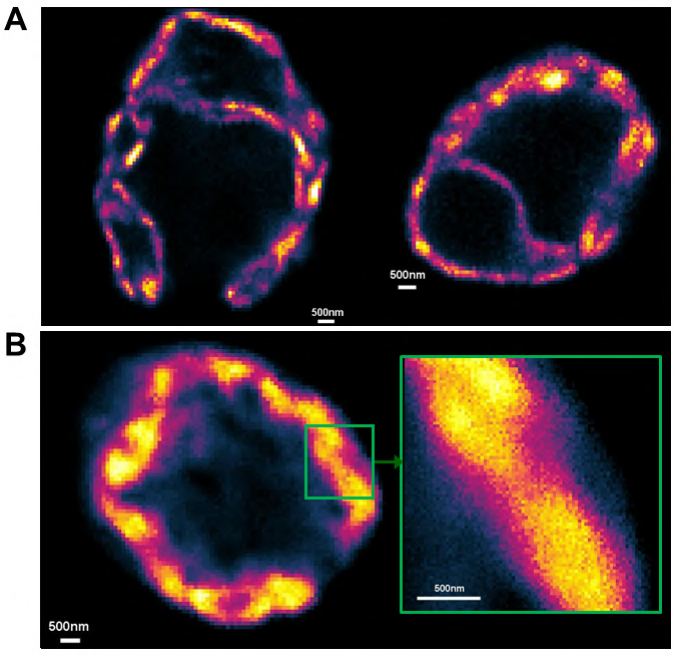

Fig. 7.4. Thylakoid organization in *Chlamydomonas r. in vivo*. (A) PRN images of two different cells from the same sample preparation. (B) PRN images of a cell scanned by 100 nm *x*&*y* steps and a ROI of the same cell scanned by 25 nm *x*&*y* steps. In panel (A) the cells were scanned by 100 nm *x*&*y* steps, with 100x objective, collecting emission in >655 nm range, in (B) – with 60x objective, collecting emission in 675-685 nm range; samples were excited at 488 nm.

Using PRN, it is possible to observe thylakoid architecture near the surface of the cell by adjusting the focal plane which is usually difficult to obtain by EM techniques. In Fig. 7.5A the middle and the edge planes of the cell obtained by PRN are shown, as well as the similar

experiment performed by 3D-SIM[21] (Fig. 7.5B). In 3D-SIM images some artefacts can be observed – striped pattern all over the sample, as this method uses structured grids through which the sample is scanned. *Chlamydomonas r.* are relatively big cells of approximately ten micrometers in diameter with a lens-shaped surface, which leads to an appearance of additional interference patterns and concomitant artefacts in SIM methods[21] which are not visible in PRN images.

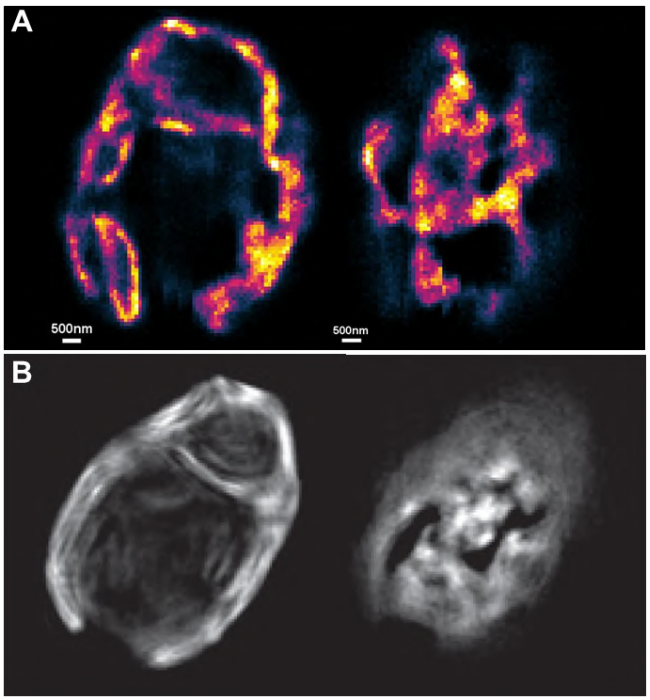

Fig. 7.5. Comparison of the PRN (A) and 3D-SIM (B) methods for *Chlamydomonas r.* imaging *in vivo*: middle planes of the cell on the left and planes close to the surface of the cell on the right. In panel (A) the cells were scanned by 100 nm *x*&*y* steps, with 100x objective, collecting emission in >655 nm range; samples were excited at 488 nm. Panel (B) is reproduced from Iwai *et al*, *The Plant Journal*, 2018[21].

7.2.4 3D reconstruction of *Chlamydomonas r.* thylakoid network *in vivo*

A *Chlamydomonas r.* cell *in vivo* scanned by PRN at several planes and the volumetric reconstruction of them are shown in Fig. 7.6. To our knowledge, these images are the first 3D reconstruction of the *in vivo* thylakoid membrane organization in *Chlamydomonas r*. From the cross-sections of the 3D image taken every 45 degrees while rotating it around *y* axis (7.6B), a continuous thylakoid network with occasional non-fluorescent spaces can be observed. Also, a big spherical non-fluorescent volume in the middle of the cell which corresponds to the pyrenoid place is visible. Such random patterns make membrane organization at many focal planes in 2D images appear very different. Fig. 7.6C shows the cross-sections at every 200 nm going from

the front into the depth of the cell, which enables us to follow the thylakoid network changes through the sample. It is observed that some patches actually resemble round grana-like disks with less intense interconnections between them – stroma lamellae-like structures. As for plant chloroplasts, it is the same situation with the algae cell orientation – they are always laying on the surface in a particular direction, and thus to observe the cell from the side, 3D reconstruction is a solution.

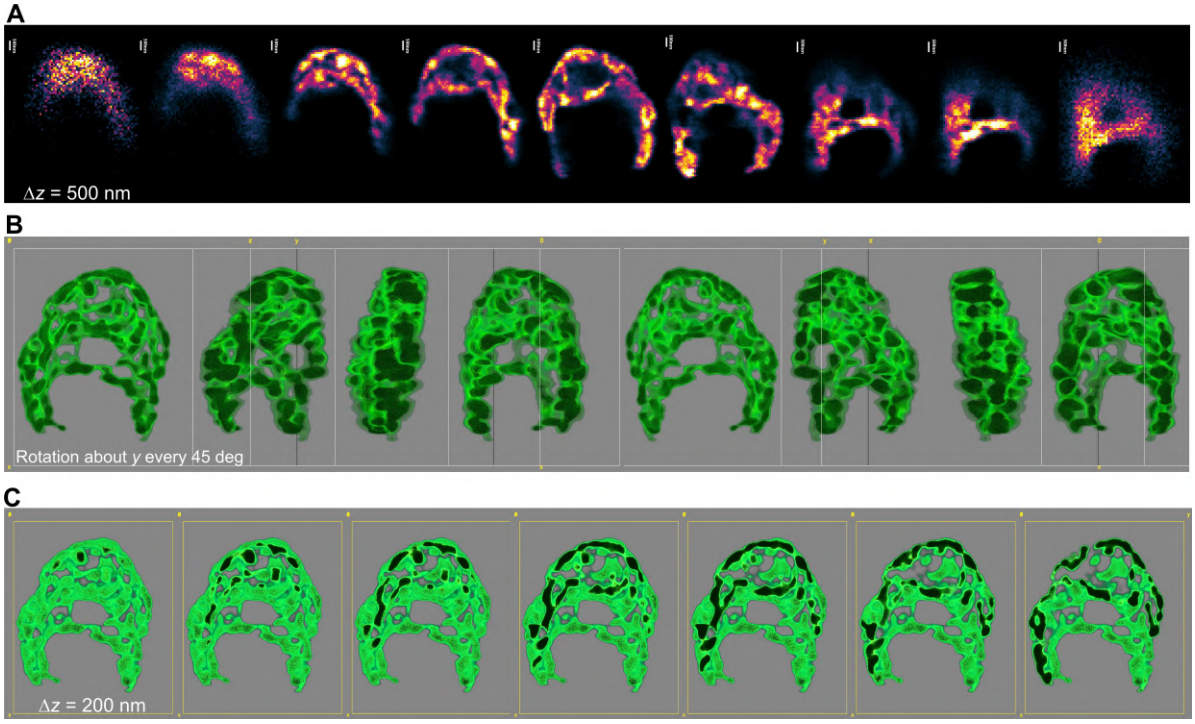

Fig. 7.6. (A) An axial scan of *Chlamydomonas r.* cell *in vivo* by PRN. (B) Cross-sections of the 3D reconstruction of *Chlamydomonas r.* cell every 45 degrees rotating it around *y* axis. (C) Cross-sections of the 3D reconstruction from the front view every 200 nm in *z* direction. In panel (A), scale bar at the top left corner of the images is 500 nm. Cell was scanned by 50 nm *x&y* steps, and 500 nm *z* steps, with 100x objective, collecting emission in >655 nm range; sample was excited at 488 nm.

7.2.5 Thylakoid organisation in diatoms

Imaging of diatoms is challenging as they differ greatly in their size and shape; some possess only a few plastids inside the cell, for example, pennate diatoms *Phaeodactylum t.*[13] or *Amphora veneta*[29], and some – several plastids in the case of the centric diatoms *Thalassiosira pseudonana* (*p.*)[30,31]. As was shown before, PRN enables us to image relatively large samples. The thylakoid organisation in this section is presented for two species of centric diatoms which differ in size and the number of plastids per cell. First, *Cyclotella meneghiniana* (*m.*) diatoms – they are more than 10 μm in diameter, and have around a dozen of plastids inside. Second, *Thalassiosira pseudonana* (*p.*) – smaller in size and possessing fewer plastids in the silica-

based shell. Fig. 7.7 shows conventional microscopy images obtained for both species *in vivo*. In white light (WL) images (Fig. 7.7A and C, left), the silica shell of the diatom cells can be observed (marked with the green arrow). In the WL image of *Thalassiosira p.* we can see two cells – one laying on the side of the cylinder and another – on the base. The same situation is shown in EM images in Fig. 7.7B. In the WL image of *Cyclotella m.* two cells are observed as well, both laying on the side surface. Epi-fluorescence (EF) images (Fig. 7.7A and C, right) register thylakoid emission coming from the plastids inside the cells. It can be seen that *Thalassiosira p.* has only a few plastids, meanwhile, *Cyclotella m.* possess many densely packed plastids.

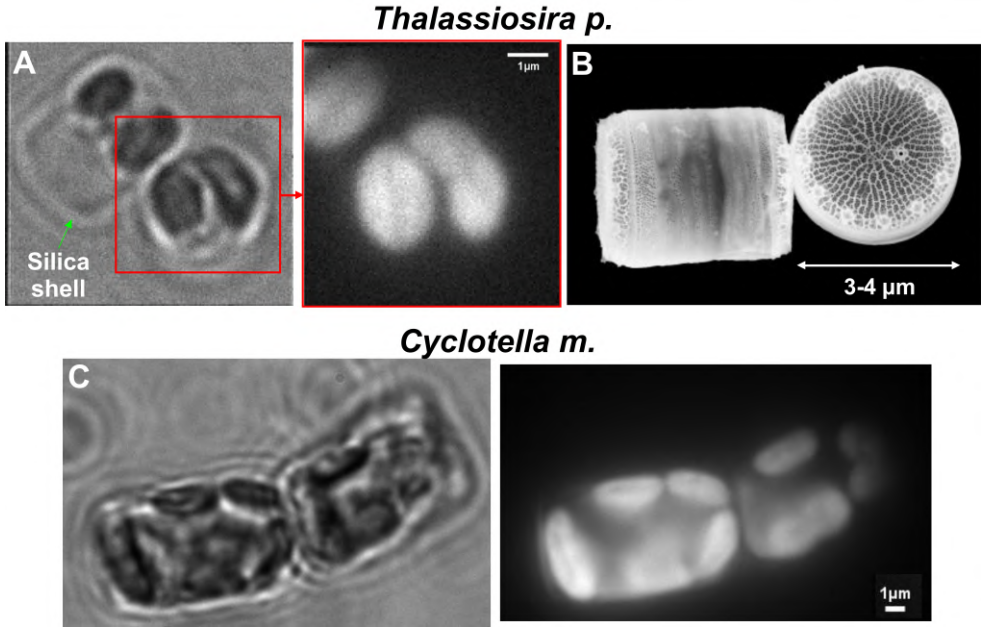

Fig. 7.7. Conventional microscopy of diatoms *in vivo*. (A) *Thalassiosira p.:* wide-field white-light image on the left, the ROI from this image obtained by epi-fluorescence microscopy on the right. (B) EM image of *Thalassiosira p.* showing the cell on the side and from the top. The cylindric structure is also similar for *Cyclotella m.* with a larger diameter (by few micrometers). (C) *Cyclotella m.:* wide-field white-light image on the left, and same image obtained by epi-fluorescence microscopy on the right. For epi-fluorescence the sample was excited at *ca.* 488 nm and emission was collected in 660-700 nm range. (B) Image courtesy of N. Kröger, Georgia Institute of Technology, Atlanta

Fig. 7.8 shows, to our knowledge, the first high-resolution 3D reconstruction of the thylakoid network in a *Cyclotella m.* cell *in vivo*. The cell was scanned at five *z*-planes which were reconstructed to obtain a membrane system for half of the volume of the cell (Fig. 7.8A, B). An interesting arrangement of the plastids in the shell can be noticed. They are always concentrated at the shell wall – same as for plant chloroplasts in mesophyll cells[32]. Also, it is observed that plastids vary in size even within the same cell, as well as differences in the size from cell to cell in the same sample, which is determined by their growth phase[33]. The non-fluorescent volume in the centre of each plastid is the pyrenoid space, where it is thought to be of the shape

of a lens[15,34]. Unfortunately, due to rather homogeneous distribution of the thylakoids in the plastids, it is not possible to observe more detailed features by imaging whole cells.

Diatoms are related to algae and evolved by secondary endosymbiosis – their plastids possess four envelopes[14]. The isolation of these plastids is an extremely complex process compared to the isolation of chloroplasts from plants[14,35]. The whole cell imaging complicates the visualization of the separate plastids. Therefore, for better insight into the plastid thylakoid structure, their isolation should be optimised to preserve as closely as possible their native state. This isolation was performed as described in Materials and methods (section 7.4).

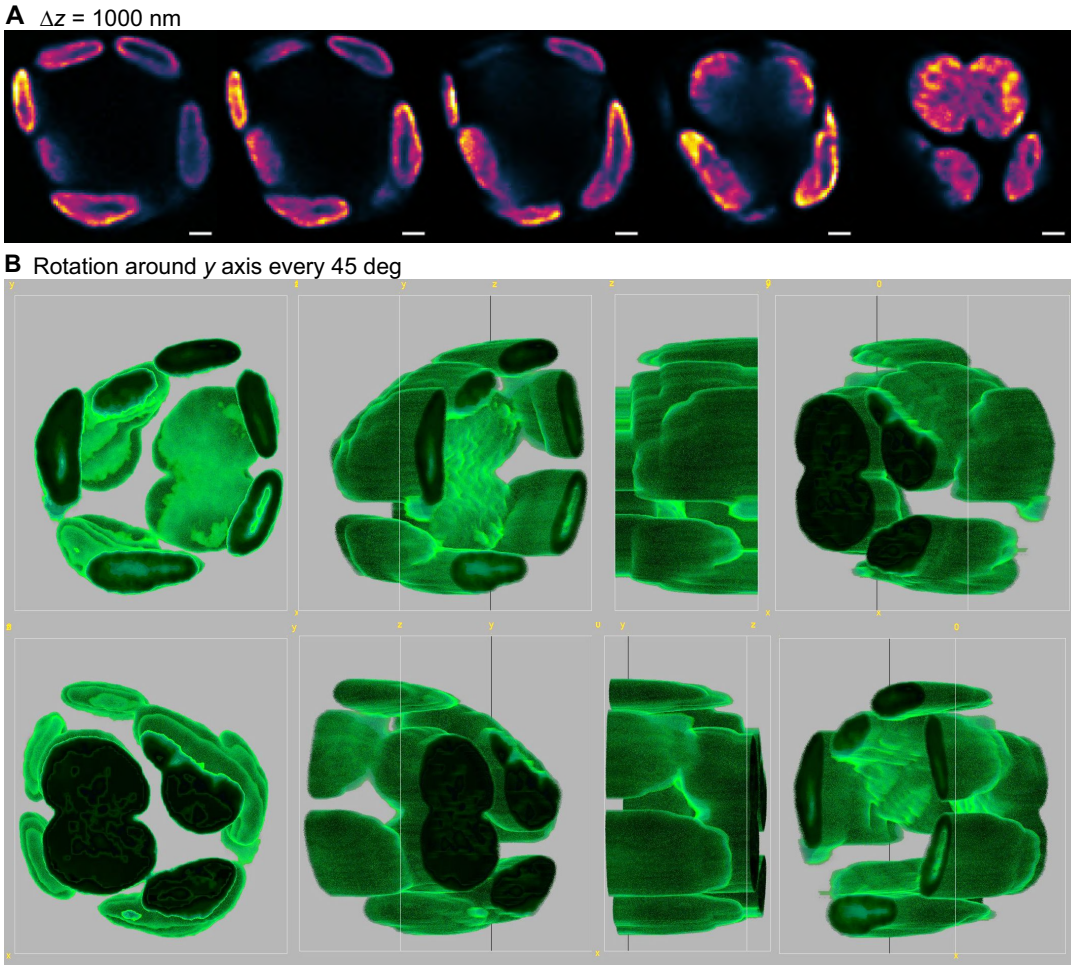

Fig. 7.8. (A) An axial scan of *Cyclotella m.* cell *in vivo* by PRN. (B) Cross-sections of the 3D reconstruction of *Cyclotella m.* cell by 45 degrees by rotating the volumetric image around y axis. In panel (A), the scale bar is 1 μm. Cell was scanned by 100 nm x&y steps, and 1000 nm z steps, with 100x objective, collecting emission in 660-700 nm range; sample was excited at 488 nm. Shown data was deconvolved as described in Materials and methods (section 6.4).

Fig. 7.9 shows PRN images of an isolated plastid scanned at several z planes and the 3D reconstruction of the obtained images. From the images, interesting features can be observed – the thin thylakoid membrane stack piercing the pyrenoid (marked with yellow arrows), which was observed in EM images for other diatom species[13,15,29,35,36] and in SIM by using labelling[36].

Thylakoids penetrating the pyrenoid are reported to be important for the photosynthetic efficiency as they facilitate the CO_2 delivery to the carbon fixation reactions[36,37]. This structure is better visible from the cross-sections in z direction of the 3D reconstruction rotated by 60 degrees (Fig. 7.9B). In general, it can be also observed that half of the plastid is different in shape than that of a spherical plant chloroplast – it is more lens-shaped with a slightly higher thylakoid concentration at the narrow edges (Fig. 7.9A). Despite the fact that the thylakoid structure in diatoms appears to be very different from that of a typical plant chloroplast, it is also reported to optimize photosynthesis[1].

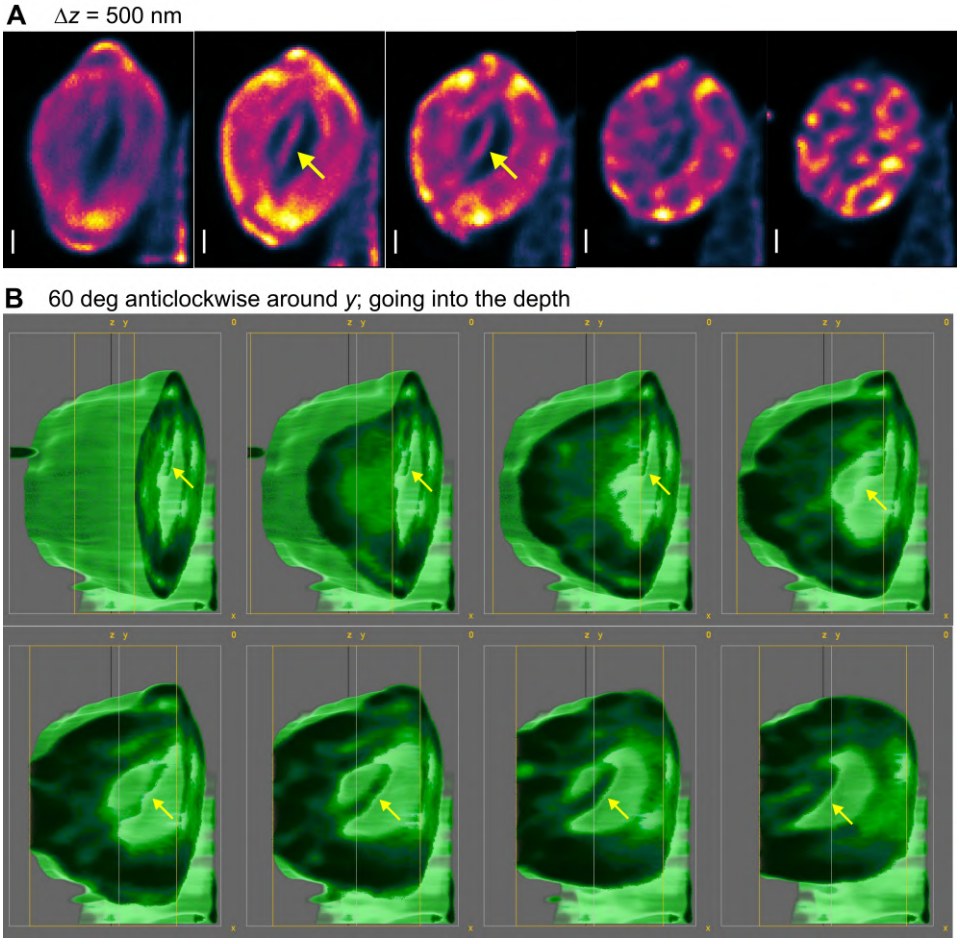

Fig. 7.9. (A) An axial scan of *Thalassiosira p.* isolated plastid by PRN. (B) Cross-sections of the 3D reconstruction in *z* direction of *Thalassiosira p.* plastid positioned at 60 deg angle. In panel (A), vertical scale bar at the bottom left corner of the images is 500 nm.The plastid was scanned by 50 nm *x&y* steps, and 500 nm *z* steps, with 100x objective, collecting emission in 660-700 nm range; sample was excited at 488 nm. Shown data was deconvolved as described in Materials and methods (section 6.4).

7.3 Conclusions

Intricate thylakoid organisation was obtained for diverse range of different photosynthetic organisms by using the high-resolution PRN method. Chlorophyll autofluorescence was recorded by scanning intact plant (pea, spinach, arabidopsis) chloroplasts, green algae (*Chlamydomonas r.*) and diatom (*Cyclotella m.*) cells *in vivo*, and isolated diatom plastids (*Thalassiosira p.*) at several z planes. The obtained 2D images were then used for the volumetric 3D reconstruction of the biologically relevant thylakoid network within the particular organism. Complex 3D thylakoid structures for green algae and diatom cells *in vivo* are the first such examples, while the structure obtained for arabidopsis is shown to be highly improved from what we can find in the current literature. Also, it was shown that grana diameters in plant chloroplasts can be evaluated, and the changes of a few tens of nanometres caused by the plant acclimation can be detected. The obtained grana diameters of 380 nm for high-light-grown plants and 420 nm for low-light plants are in a good agreement to what was reported before. The most precise results for grana estimation could be achieved performing deconvolution by systems point-spread-function (discussed in Chapter 6) on the obtained PRN images, which would result in the closest values to that of the real diameters.

From acquired thylakoid architectures for different organisms, we conclude that the highly organized grana and stroma lamellae organization in plants is not observed in *Chlamydomonas r.*, which possess a relatively similar photosynthetic apparatus. However, some stacking features could be seen in this green algae. Very different thylakoid organisation is observed in diatoms, exhibiting a rather homogeneous thylakoid distribution in their plastids. The thin stack of thylakoids penetrating the pyrenoid in the plastid of diatom was clearly visible in the PRN images, which was obtained before only by EM or fluorescence imaging using labelling.

High-resolution fluorescence imaging using PRN enables us to follow dynamics, contrary to EM. However, it is limited by the fact that one observes mainly PSII emission at physiological temperatures as the fluorescence from PSI is negligible. To observe PSI, one would need to use fluorescence labelling, which complicates sample preparation but nevertheless could give more insights into the overall thylakoid structure. Despite the obtained structures do not present the complete thylakoid organization in the organisms, they reasonably complement the high-resolution EM data. As PRN can be used for the detection of multiple emission ranges, a solution could be labelling of different compartments and non-fluorescent organelles, and building a sophisticated 3D multi-compartment structures. Furthermore, PRN imaging of the same organism under changing light/environment conditions is an attractive direction for future experiments.

7.4 Materials and methods

7.4.1 Organism growth conditions and plastid isolation

Spinach (*Spinacia oleracea*), pea (*Pisum sativum*) and arabidopsis (*Arabidopsis thaliana*) plants were grown under high-light conditions: 600 $\mu Em^{-2}s^{-1}$ of white light for 8h a day, and low-light conditions: 120 $\mu Em^{-2}s^{-1}$ of white light for 8h a day. Philips MASTER PL-L (Polar 55W/840/4P 1CT) lamps were used for plant exposure.

Plant chloroplast isolation was performed at 4°C temperature in the dark. Sliced leaves (20-30 g) were homogenised in the blender for 5 seconds in 200 ml of a medium: 300 mM sorbitol, 1 mM $MgCl_2$, 1 mM $MnCl_2$, 2 mM EDTA, 30 mM KCl, 0.5 mM KH_2PO_4 and 50 mM MES-KOH (pH = 6.1). The obtained mixture was filtered through 6 layers of cheesecloth and centrifuged at 2000g for 2 min. The pellet obtained after centrifugation was suspended in the same medium, and centrifuged again at 2000g for 2 min. The obtained pellet was resuspended in the medium: 300 mM sorbitol, 1 mM $MgCl_2$, 1 mM $MnCl_2$, 2 mM EDTA, 30 mM KCl, 0.5 mM KH_2PO_4 and 50 mM HEPES-KOH (pH = 7.6), and centrifuged at 2500g for 3 min. The obtained pellet of the intact chloroplasts was then resuspended in 1-2 ml of the same medium.

Chlamydomonas r. cells were grown in Tris-Acetate-Phosphate (TAP) medium in 25 ml Erlenmeyer flasks with 10 ml of TAP medium by shaking at 150 rpm at room temperature (20°). *Thalassiosira p. and Cyclotella m.* were cultured and their plastids isolated as described in[38].

7.4.2 Imaging system and image treatment

PRN imaging system used in this study is described in detail in section 6.4.3. A simplified scheme of the experimental set-up is shown in Fig. 7.10. All the samples presented in this chapter were excited at 488 nm, and the emission was collected by different filters: Semrock FF01-679/41-25 (660–700 nm range), Chroma ET655lp (>655 nm range), and Thorlabs FB680-10 (675–685 nm range), depending on the experiment. Emission was registered by an EMCCD camera (Andor, Belfast, UK). Super-resolution fluorescence image reconstruction was performed, as described in Chapter 6. Samples were scanned by 25-1000 nm *x*, *y*&*z* steps. Images were post-processed, as described in section 6.4.4.

Samples were prepared as follows: 5 µl of the sample was sandwiched in between two round cover-slips and sealed with nail polish. The bottom glass was coated with Corning® Cell-Tak™ to attach cells to the glass and inhibit their movement.

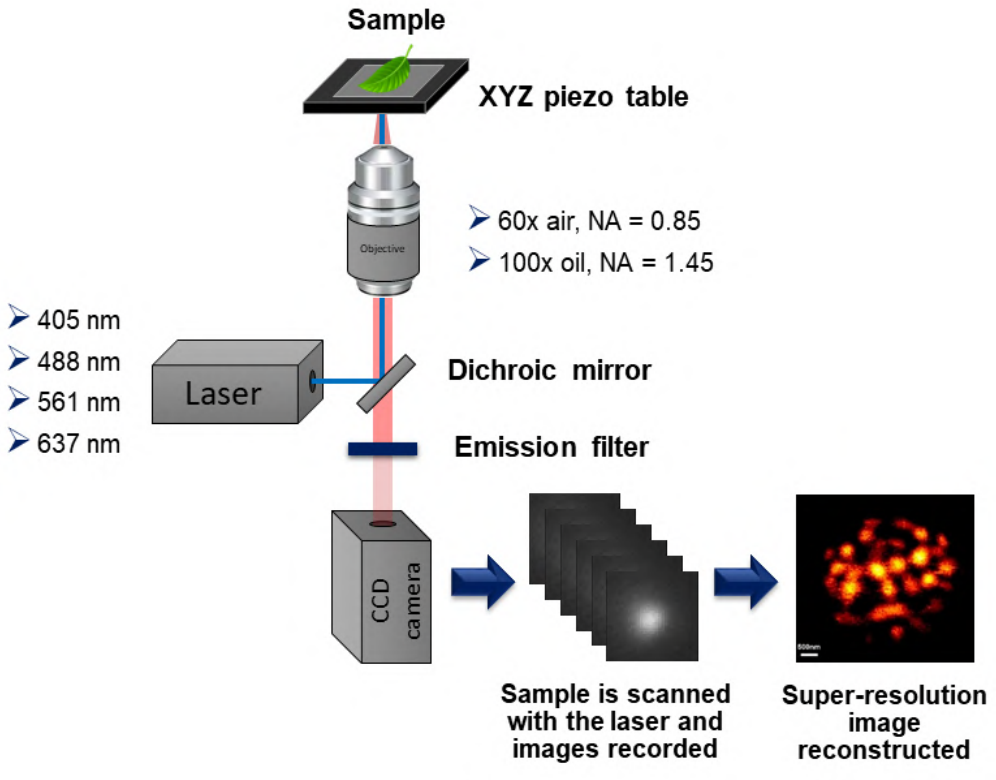

Fig. 7.10. Simplified scheme for the experimental PRN system.

7.4.3 Grana diameter evaluation

The scheme for grana diameter evaluation for plant chloroplasts is shown in Fig. 7.11. Firstly, one grana was selected from the whole chloroplast PRN image and fitted by a Gauss 2D function:

$$z = z_0 + A\exp[-0.5((x-xc)/w_1)^2 - 0.5((y-yc)/w_2)^2]. \quad (7.1)$$

Secondly, the grana diameter was determined as FWHM of the Gauss 2D fit of the obtained granum image. All the grana diameters were evaluated from the intact chloroplasts isolated from the plants under the same conditions for HL and LL cases. Only upper young leaves of the plants were used for chloroplast isolation, and imaging conditions were identical: 100x oil objective, 488 nm laser excitation, 660-700 nm emission range, 50 nm $x\&y$ scanning step sizes. Around 50 grana stacks were evaluated from several chloroplasts for each of the plant growth conditions.

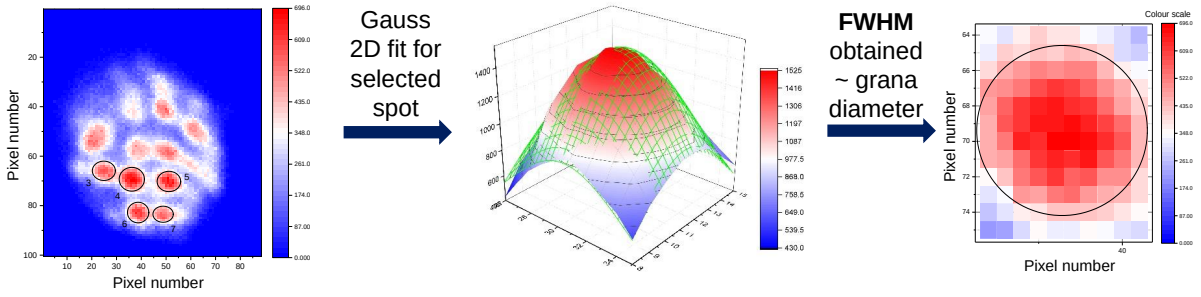

Fig. 7.11. Plant chloroplast grana diameter evaluation steps.

Acknowledgements

I would like to thank to Dr. Anja Krieger-Liszkay (CEA Paris-Saclay, France) for teaching and consulting on plant cultivation methods and chloroplast isolation procedures; to Dr. Francesca Zito (Institut de Biologie Physico-Chimique (IBPC), France) for providing *Chlamydomonas r.,* and teaching how to maintain and culture them; to Prof. Dr. Claudia Büchel and Claudio Calvaruso (Institute of Molecular Biosciences, University of Frankfurt) for providing diatoms *Cyclotella m.* and *Thalassiosira p.*, and teaching how to maintain and culture them, as well as plastid isolation methods.

References

[1] S. Flori, P. H. Jouneau, B. Bailleul, *et al.*, "Plastid thylakoid architecture optimizes photosynthesis in diatoms," *Nature Communications*, 2017, **8**.

[2] H. D. Tauschel and G. Drews, "Thylakoidmorphogenese bei *Rhodopseudomonas palustris*," *Archiv für Mikrobiologie*, 1967, **59**, 381–404.

[3] D. J. Paolillo, "The three-dimensional arrangement of intergranal lamellae in chloroplasts.," *Journal of Cell Science*, 1970, **6**, 243–255.

[4] Y. Bussi, E. Shimoni, A. Weiner, *et al.*, "Fundamental helical geometry consolidates the plant photosynthetic membrane," *Proceedings of the National Academy of Sciences of the United States of America*, 2019, **116**, 22366–22375.

[5] S. Bellaflore, F. Barneche, G. Peltler, and J. D. Rochalx, "State transitions and light adaptation require chloroplast thylakoid protein kinase STN7," *Nature*, 2005, **433**, 892–895.

[6] F. Zito, G. Finazzi, R. Delosme, W. Nitschke, D. Picot, and F. A. Wollman, "The Qo site of cytochrome b6f complexes controls the activation of the LHCII kinase," *EMBO Journal*, 1999, **18**, 2961–2969.

[7] L. C. Mackinder, C. Chen, R. D. Leib, *et al.*, "A spatial interactome reveals the protein organization of the algal CO2-concentrating mechanism," *Cell*, 2017, **171**, 133–147.e14.

[8] M. T. Meyer, C. Whittaker, and H. Griffiths, "The algal pyrenoid: key unanswered questions," *Journal of experimental botany*, 2017, **68**, 3739–3749.

[9] I. Ohad, P. Siekevitz, and G. E. Palade, "Biogenesis of chloroplast membranes," *The Journal of cell biology*, 1967, **35**, 521–552.

[10] P. A. Salomé and S. S. Merchant, "A series of fortunate events: Introducing chlamydomonas as a reference organism," *Plant Cell*, 2019, **31**, 1682–1707.

[11] B. D. Engel, M. Schaffer, L. K. Cuellar, E. Villa, J. M. Plitzko, and W. Baumeister, "Native architecture of the chlamydomonas chloroplast revealed by in situ cryo-electron tomography," *eLife*, 2015, **2015**, 1–29.

[12] M. M. Ghobara, N. Mazumder, V. Vinayak, and L. Reissig, "On light and diatoms: A photonics and photobiology review," in *Diatoms: Fundamentals and Applications* (J. Seckbach and R. Gordon, eds.), 129–189, Scrivener Publishing LLC 129, 2019.

[13] S. Flori, P. H. Jouneau, G. Finazzi, E. Maréchal, and D. Falconet, "Ultrastructure of the periplastidial compartment of the diatom *Phaeodactylum tricornutum*," *Protist*, 2016, **167**, 254–267.

[14] A. F. Schober, S. Flori, G. Finazzi, P. G. Kroth, and C. Bártulos, "Isolation of plastid fractions from the diatoms Thalassiosira pseudonana and *Phaeodactylum tricornutum*,"

in *Plastids. Methods in Molecular Biology* (E. Maréchal, ed.), vol. 1829, 189–203, New York: Humana Press, 2018.

[15] A. Jenks and S. P. Gibbs, "Immunolocalization and distribution of form II Rubisco in the pyrenoid and chloroplast stroma of *Amphidinium Carterae* and form I Rubisco in the symbiont-derived plastids of *Peridinium Foliaceum* (Dinophyceae)," *J. Phycol.*, 2000, **36**, 127–138.

[16] I. Rumak, R. Mazur, K. Gieczewska, *et al.*, "Correlation between spatial (3D) structure of pea and bean thylakoid membranes and arrangement of chlorophyll-protein complexes," *BMC Plant Biology*, 2012, **12**, 1–18.

[17] J. R. Austin and L. A. Staehelin, "Three-dimensional architecture of grana and stroma thylakoids of higher plants as determined by electron tomography," *Plant Physiology*, 2011, **155**, 1601–1611.

[18] E. Hummel, P. Guttmann, S. Werner, *et al.*, "3D ultrastructural organization of whole *Chlamydomonas reinhardtii* cells studied by nanoscale soft X-Ray tomography," *PLoS ONE*, 2012, **7**.

[19] M. Beck and W. Baumeister, "Cryo-electron tomography: can it reveal the molecular sociology of cells in atomic detail?," *Trends in Cell Biology*, 2016, **26**, 825–837.

[20] M. Iwai, M. Yokono, K. Kurokawa, A. Ichihara, and A. Nakano, "Live-cell visualization of excitation energy dynamics in chloroplast thylakoid structures," *Scientific Reports*, 2016, **6**, 1–10.

[21] M. Iwai, M. S. Roth, and K. K. Niyogi, "Subdiffraction-resolution live-cell imaging for visualizing thylakoid membranes," *Plant Journal*, 2018, **96**, 233–243.

[22] W. H. J. Wood, C. MacGregor-Chatwin, S. F. H. Barnett, *et al.*, "Dynamic thylakoid stacking regulates the balance between linear and cyclic photosynthetic electron transfer," *Nature Plants*, 2018, **4**, 116–127.

[23] M. Herbstová, S. Tietz, C. Kinzel, M. V. Turkina, and H. Kirchhoff, "Architectural switch in plant photosynthetic membranes induced by light stress," *Proceedings of the National Academy of Sciences of the United States of America*, 2012, **109**, 20130–20135.

[24] S. Puthiyaveetila, O. Tsabarib, T. Lowryc, S. Lenhertc, R. R. Lewisd, Z. Reichb, and H. Kirchhoffa, "Compartmentalization of the protein repair machinery in photosynthetic membranes," *Proceedings of the National Academy of Sciences of the United States of America*, 2014, **111**, 15839–15844.

[25] I. Rumak, K. Gieczewska, B. Kierdaszuk, W. I. Gruszecki, A. Mostowska, R. Mazur, and M. Garstka, "3-D modelling of chloroplast structure under (Mg2+) magnesium ion treatment. Relationship between thylakoid membrane arrangement and stacking," *Biochimica et Biophysica Acta - Bioenergetics*, 2010, **1797**, 1736–1748.

[26] L. Mustárdy and G. Garab, "Granum revisited. A three-dimensional model - Where things fall into place," *Trends in Plant Science*, 2003, **8**, 117–122.

[27] L. Mustárdy, K. Buttle, G. Steinbach, and G. Garab, "The three-dimensional network of the thylakoid membranes in plants: Quasihelical model of the granum-stroma assembly," *Plant Cell*, 2008, **20**, 2552–2557.

[28] U. W. Goodenough and L. A. Staehelin, "Structural differentiation of stacked and unstacked chloroplastmembranes: Freeze-etch electron microscopy of wild-type and mutant strains of *Chlamydomonas*," *Journal of Cell Biology*, 1971, **48**, 594–619.

[29] G. F. Daniel, A. H. Chamberlain, and E. B. Jones, "Ultrastructural observations on the marine fouling diatom *Amphora*," *Helgoländer Meeresuntersuchungen*, 1980, **34**, 123–149.

[30] P. Gröger, N. Poulsen, J. Klemm, N. Kröger, and M. Schlierf, "Establishing super-resolution imaging for proteins in diatom biosilica," *Scientific Reports*, 2016, **6**, 1–8.

[31] A. Kotzsch, P. Gröger, D. Pawolski, P. H. H. Bomans, N. A. J. M. Sommerdijk, M. Schlierf, and N. Kröger, "Silicanin-1 is a conserved diatom membrane protein involved in silica biomineralization," *BMC Biology*, 2017, **15**, 9–11.

[32] T. Uwada, L. T. Huang, P. Y. Hee, A. Usman, and H. Masuhara, "Size-dependent optical properties of grana inside chloroplast of plant cells," *Journal of Physical Chemistry B*, 2017, **121**, 915–922.

[33] E. R. Moore, B. S. Bullington, A. J. Weisberg, Y. Jiang, J. Chang, and K. H. Halsey, "Morphological and transcriptomic evidence for ammonium induction of sexual reproduction in Thalassiosira pseudonana and other centric diatoms," *PLoS ONE*, 2017, **12**, 1–18.

[34] Y. Tsuji, K. Nakajima, and Y. Matsuda, "Molecular aspects of the biophysical CO2-concentrating mechanism and its regulation in marine diatoms," *Journal of experimental botany*, 2017, **68**, 3763–3772.

[35] A. F. Schober, C. Río Bártulos, A. Bischoff, B. Lepetit, A. Gruber, and P. G. Kroth, "Organelle studies and proteome analyses of mitochondria and plastids fractions from the diatom *Thalassiosira pseudonana*," *Plant and Cell Physiology*, 2019, **60**, 1811–1828.

[36] S. Kikutani, K. Nakajima, C. Nagasato, Y. Tsuji, A. Miyatake, and Y. Matsuda, "Thylakoid luminal Θ-carbonic anhydrase critical for growth and photosynthesis in the marine diatom *Phaeodactylum tricornutum*," *Proceedings of the National Academy of Sciences of the United States of America*, 2016, **113**, 9828–9833.

[37] Y. Matsuda, K. Nakajima, and M. Tachibana, "Recent progresses on the genetic basis of the regulation of CO2 acquisition systems in response to CO2 concentration," *Photosynthesis Research*, 2011, **109**, 191–203.

[38] C. Calvaruso, A. Rokka, E. M. Aro, and C. Büchela, “Specific Lhc proteins are bound to PSI or PSII supercomplexes in the diatom *Thalassiosira pseudonana*,” *Plant Physiology*, 2020, **183**, 67–79.